JOURNAL OF MATERIALS SCIENCE **40** (2005) 5999–6005

The effect of grain size on the flow stress determined from spherical microindentation of die-cast magnesium AM60B alloy

J. P. WEILER*, J. T. WOOD, R. J. KLASSEN
Department of Mechanical and Materials Engineering, University of Western Ontario, London, Ontario, Canada, N6A 5B9
E-mail: jpweiler@uwo.ca

R. BERKMORTEL, G. WANG
Meridian Technologies Inc., 25 MacNab Ave., Strathroy, Ontario, Canada, N7G 4H6

Published online: 8 September 2005

Spherical microindentation tests were performed on samples cut from an AM60B magnesium alloy die casting to determine the effects of grain size on the local flow stress. Five samples were indented in the skin region (finer grain sizes), two samples in the core region (larger grain sizes and dendrites), and one sample was indented in both the skin and core region of the die-casting. It was determined that the Hall-Petch equation is applicable for predicting the initial yield point and the flow stress at several levels of plastic strain only in the skin region, and not the core region, of the die-casting. The Hall-Petch slope and intercept stress, determined from spherical indentation in the skin region, compare accurately with previously published results. Possible reasons for indentation results from the core region deviating from the Hall-Petch relationship are discussed. The Hall-Petch slope follows a linearly increasing relation with the square root of plastic strain; however, no conclusions can be drawn concerning this because of the small range of plastic strain tested.

1. Introduction

In this paper, the local properties of AM60B are investigated by spherical microindentation. The effect of varying grain size on the local flow stress calculated from spherical indentation is determined, in both the refined grain size skin region and in the larger grain size core region of the die-casting. Further, the applicability and the parameters of the Hall-Petch equation relating the local flow stress to the average measured grain size are determined.

The Hall-Petch equation [1, 2] expresses the flow stress, σ, of a material as a function of the grain size, d, as:

$$\sigma = \sigma_o + kd^{-1/2} \tag{1}$$

where σ_o is the intercept stress and k is the Hall-Petch slope. The Hall-Petch equation has also been used in the past to relate the measured hardness during spherical indentation to the grain size of a material [3]. Since the grain size is controlled by the cooling rate, variation in grain size occurs throughout a typical metal casting, particularly in the case of complex die-castings where the cooling rates depend on the thickness of the cross-section.

In the case of die-cast magnesium components, a region of refined grains, referred to as the skin region, exists near the surface of the casting. The thickness of this 'skin' region ranges from 50–500 μm [4]. Larger grains exist in the core of the casting. The core region also contains a greater concentration of defects, such as inclusions and porosity [4], as shown in Fig. 1. In this investigation, spherical indentation is used to measure the dependence of the local flow stress upon the local grain size in a magnesium die-casting. The average grain sizes in the skin and core regions of the die-casting magnesium alloy AM60B studied here were previously reported to be approximately 7 and 17 μm, respectively [5].

2. Spherical indentation

The technique to evaluate the hardness of materials using spherical indentation was first introduced by Brinell (see [6]). It was further improved upon by O'Neill [7] and Tabor [8], who demonstrated that the average

*Author to whom all correspondence should be addressed.
0022-2461
DOI: 10.1007/s10853-005-1295-2

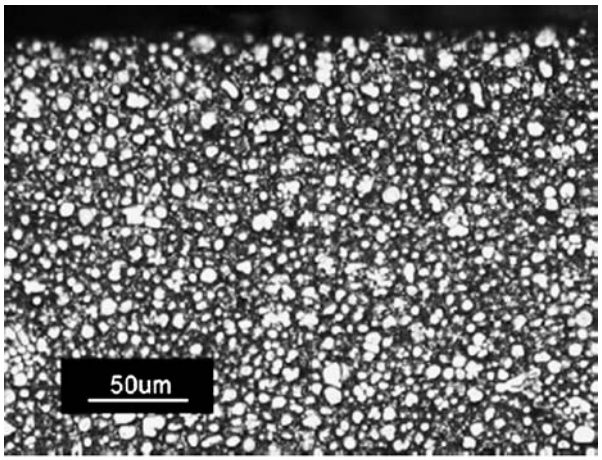

(a)

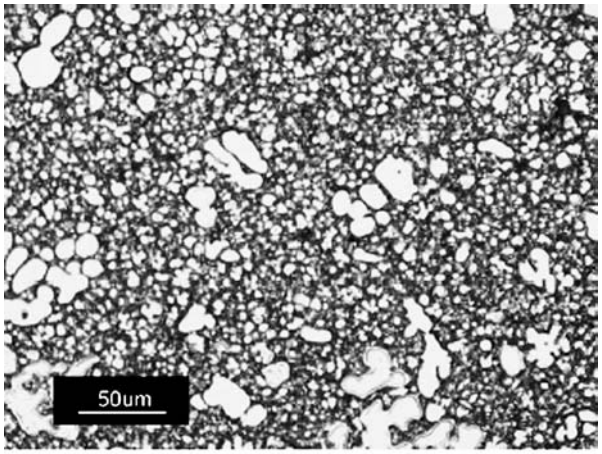

(b)

Figure 1 Typical microstructures of the skin (a), and core (b), regions of the die cast magnesium alloy AM60B. Fig. 1a shows a consistent region of refined grains, which is typical of Samples I–VI (Table II). Fig. 1b shows larger grains, several very large dendrites and regions of microporosity, which is typical of Samples VI–VIII.

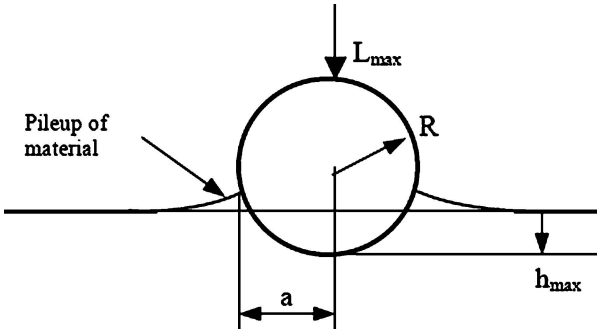

Figure 2 Schematic diagram of the indentation of a ductile material by a rigid sphere of radius R under an applied load, L_{max}.

indentation strain, ε_{avg}, was a function of the ratio a/R, where a is the indentation radius and R is the radius of the spherical indenter (Fig. 2). Several studies [8–10] have presented theories that relate the mean contact pressure, P_M, during spherical indentation to the flow stress in uniaxial tension. The implication of these findings is that the tensile flow curve can be deduced from indentation tests performed to various ratios of a/R [11–13]. Spherical micro-indentation, using indenters less then 1 mm in radius, can therefore be used to measure the effects of microstructure on the local flow stress of a material. The grain size influence on the indentation hardness of a number of materials has already been studied [4, 14–17].

What follows is a summary of the theory, and the equations developed, that relate the average flow stress and plastic strain during spherical indentation to the parameters of indentation load and depth.

2.1. The indentation contact radius, *a*

The indentation contact radius is related to the plastic indentation depth, h_c, and a dimensionless constant, c, which represents the amount of sink-in or pileup around the indentation. The parameter h_c, can be determined at any point during an indentation test by performing a partial unloading of the indenter. When the spherical shape of the indenter is taken into account, h_c, can be expressed as [11, 18]:

$$h_c = \frac{1}{4}(h_{\max} + 3h_i) \tag{2}$$

where h_{max} is the indentation depth prior to the partial unloading, and h_i is the indentation depth extrapolated to zero load along the initial slope of the unloading curve [18].

The occurrence of material pileup or sink-in around the indenter will affect the actual indentation contact radius and is a function of the strain-hardening exponent, n, of the indented material. The following expression for the parameter, c, is widely used to account for the effect of pileup or sink-in during indentation [19]:

$$c = \frac{5(2-n)}{2(4+n)} = \left[\frac{a}{a^*}\right]^2 \tag{3}$$

In this expression, a^* is the indentation contact radius without the consideration of the effects of pileup or sink-in. The actual contact radius is then given as [11]:

$$a = \sqrt{c\left(2Rh_c - h_c^2\right)} \tag{4}$$

2.2. The average indentation stress and strain

The average plastic strain, ε_{avg}, around a spherical indentation is a function of the ratio a/R. Tabor suggested, based upon experimentation, that [8]:

$$\varepsilon_{avg} = 0.2\frac{a}{R} \tag{5}$$

and this expression is widely accepted, and we, therefore, use it to determine ε_{avg} in this study. The mean contact pressure, P_M during indentation is given by [8]:

$$P_M = \frac{L}{\pi a^2} \tag{6}$$

where L is the indentation load.

The average indentation stress, σ_{avg}, around a spherical indentation is a function of P_M, and a constraint

TABLE I Chemical composition of the AM60B alloy in wt%

Alloy	Al	Mn	Zn	Si	Cu	Ni	Fe	Mg
AM60B	5.5–6.5	0.22–0.6	0.22 Max	0.1 Max	0.01 Max	0.002 Max	0.005 Max	Balance

factor, Ψ [8]:

$$\sigma_{\text{avg}} = \frac{P_M}{\Psi} \tag{7}$$

The constant Ψ depends upon the plasticity of the deforming material and the shape of the indenter. The dependence of Ψ upon plasticity can be expressed in terms of the following plasticity parameter, ϕ, proposed by Johnson [9]:

$$\phi = \frac{E^*}{\sigma_y}\frac{a}{R} \tag{8}$$

where E^* is a modified Young's modulus ($E^* = E/1-\nu^2$), ν is Poisson's ratio, and σ_y is the yield stress of the material. When ϕ is less then 2, spherical indentation occurs primarily through elastic deformation. When ϕ is greater then 100, spherical indentation occurs primarily by fully plastic deformation. When ϕ is between 2 and 100, the deformation process involves significant elastic and plastic deformation. In this region Mesarovic and Fleck [10] have proposed that $\Psi$is non-linearly dependent upon ϕ (see Fig. 7 in Ref. [10]).

In the spherical indentation tests that follow, the deformation conditions result in ϕ being between 2 and 100; therefore, the non-linear relation between Ψ and ϕ, proposed by Mesarovic and Fleck is used to determine σ_{avg} from P_M (see Section 4).

3. Experimental procedures

3.1. Test material

Spherical microindentation tests were performed in the skin region of five samples, in the core region of two samples, and in both the skin and the core regions of one sample, taken from different locations in an AM60B magnesium alloy die-casting thin-walled (3.0 $\pm$ 0.1 mm) component. The chemical composition of the AM60B alloy is given in Table I. The average grain size, d, 0.2% yield strength, σ_y, and ultimate tensile strength, σ_{UTS}, of each sample are shown in Table II [20, 21]. The grain sizes shown were determined using optical microscopy, at a magnification of 200X, and digital image analysis. These measurements were performed using the intercept length method based on ASTM Designation E1382-97 [20]. The average grain sizes shown in Table I were determined as the average of three separate fields of measurement on each sample. Each field of measurement in the grain size analysis sampled a range of 600–1300 grains [20]. The distributions of the measured grain sizes in Samples I and VI-Core are shown in Fig. 4. The microstructures of typical skin and core regions are shown in Fig. 1.

A typical tensile stress-strain curve of the magnesium alloy AM60B component tested in this study is shown in Fig. 3 [21]. The yielding and strain hardening characteristics observed in Fig. 3 are similar throughout the different regions of the die-cast component mechanically tested [22].

Each sample was prepared for indentation testing by polishing the as-cast surface in slurries of 1μm and, finally, 0.05 μm colloidal Al_2O_3. In the case of the core samples, VI-Core, VII, and VIII (Table II), the skin region was removed by grinding with 600 grit SiC paper, prior to polishing.

3.2. Indentation testing

The indentation tests were performed with a Micro Materials (Wrexham, U.K.) microindentation hardness tester. This instrument is computer controlled and is capable of performing multiple load-unload indentation tests with continuous acquisition of the indentation load and depth. A high-carbon steel sphere of 0.795 mm radius was used to indent the samples. The indentations

TABLE II Average grain sizes and bulk tensile stresses of each sample tested in this study. Samples I–V were indented in the skin region, Samples VII and VIII were indented in the core region, and Sample VI was indented in both the skin and the core region of the die cast magnesium alloy

Sample	Features	Average grain size, d (μm) [20]	0.2% Yield stress, σ_y (MPa) [21]	Bulk tensile stress, σ_{UTS} (MPa) [21]
I	Very refined grains	4.8	117	241
II	Refined grains	6.3	108	172
III	Small dendrites away from surface Amounts of porosity	7.3	115	175
IV	Regions of porosity	8.9	113	166
V	No significant features	9.0	103	220
VI-Skin	Small dendrites near surface	8.0	101	235
VI-Core	Very large dendrites	14.9	101	
VII	Regions of porosity Dendrites	13.9	110	197
VIII	Dendrites Regions of porosity	12.7	110	161
Casting Average		6.2 – Skin region 13.9 – Core region	112	198

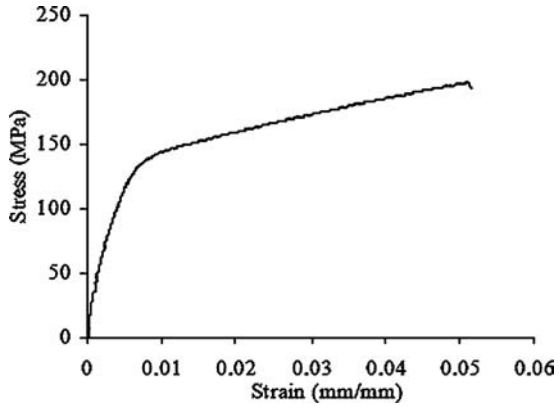

Figure 3 The typical stress-strain curve observed during mechanical testing of numerous regions of the die-cast AM60B component.

were performed with loading and unloading rates of 200 mN/s. Eight partial unloadings were performed during each indentation test. The maximum indentation load achieved during each test was 20 N. Four indentations were made on each sample. Fig. 5 shows two indentations performed on the surface of Sample I.

4. Experimental results

Fig. 6 shows the resulting load-depth curves of typical indentation tests performed on Samples I and VI-Core. The skin region (Sample I) has considerably higher indentation hardness than the core region (Sample V-Core). The contact radius, a, as described in 2.1, was calculated using both the load-depth curve of each partial unloading and a strain-hardening exponent of $n = 0.23$ (where the tensile curve is of the constitutive form $\sigma = K\varepsilon^n$). This strain-hardening exponent is typical of that during uniaxial tensile testing of the die-cast magnesium alloy AM60B [21, 22].

The average indentation flow stress, σ_{avg}, was calculated using Equation 7, where the constraint factor, Ψ, is a function of the plasticity parameter, ϕ [9], (as in (Fig. 7 Ref. [10]). The plasticity parameter, ϕ, of the material in this study was found to vary from 18 to 88. Within this range, the Ψ-ϕ relation can be linearly approximated as:

$$\Psi = 1.3 + 0.0037\phi \tag{9}$$

Plots of σ_{avg} vs. ε_{avg} for all of the samples tested are shown in Fig. 7. Fig. 7a shows the samples tested in the skin region, while Fig. 7b shows the samples tested in the core region. The different flow response of the samples suggests that there exist variations in both the magnitude of σ_{avg}, for a given level of ε_{avg}, and the strain-hardening exponent, which are due to microstructural differences between the samples. Further, Fig. 7 shows Sample II, with a grain size very near to the average obtained in the skin region results in stress-strain flow characteristics very similar to the stress-strain curve shown in Fig. 3.

Fig. 8 shows the approximate initial yield stress, $\sigma_{avg(y)}$, plotted versus $d^{-1/2}$. $\sigma_{avg(y)}$ was obtained by extrapolating the σ_{avg} vs. ε_{avg} trends in Fig. 7. The power law functions were linearly extrapolated to $\varepsilon_{avg} = 0$ (i.e., zero plastic strain) representing an initial yield stress. The samples indented in the skin region follow closely the dependence of $\sigma_{avg(y)}$ upon grain size predicted by the Hall-Petch equation (Equation 1). This is in accordance with other published results that demonstrate that both a magnesium-zinc alloy [23] and the die-cast magnesium alloy AZ91 [17] also exhibit a well-defined Hall-Petch relationship. The samples indented in the core region do not follow the same Hall-Petch relationship established in the skin region.

5. Discussion

5.1. Microstructural influences

Fig. 7 shows a clear difference in the initial yield stress $\sigma_{avg(y)}$ of the samples tested in this study. This difference can be attributed to the differences in the microstructure of the samples. There is typically a higher aluminum content in the skin region of the castings. This is thought to be due to the formation of pre

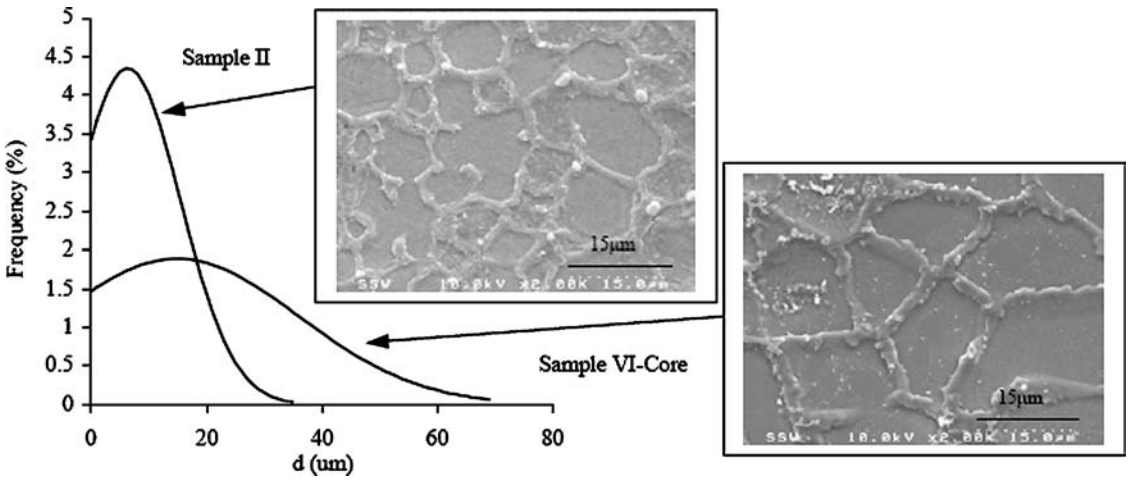

Figure 4 The frequency distribution of grain sizes measured in this study for Samples II and VI-Core indented in the skin and core regions, respectively. Scanning electron microscope images of the microstructures of Samples II and VI-Core are shown in the insets. The images show several grains in each case, approximately 4–12 μm in size for Sample II and approximately 8 to 25 μm in size for Sample VI-Core. The graph shows a distinctly wider distribution of measured grain sizes for Sample VI-Core.

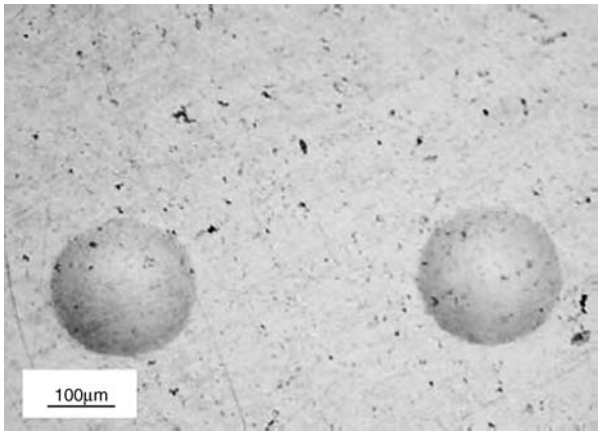

Figure 5 Two spherical indentations performed on Sample I of the AM60B die cast magnesium alloy.

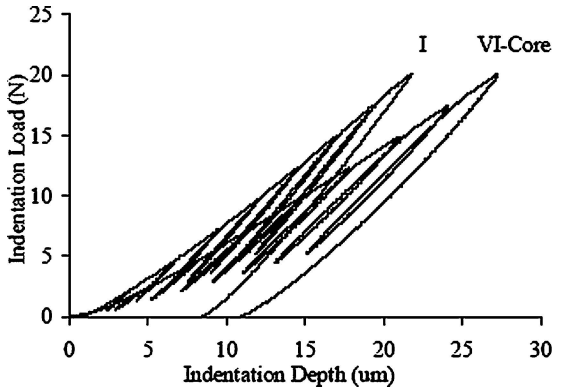

Figure 6 Load-depth curve of typical indentations performed on Sample I, in the skin region and Sample VI-Core, in the core region of the AM60B die-casting.

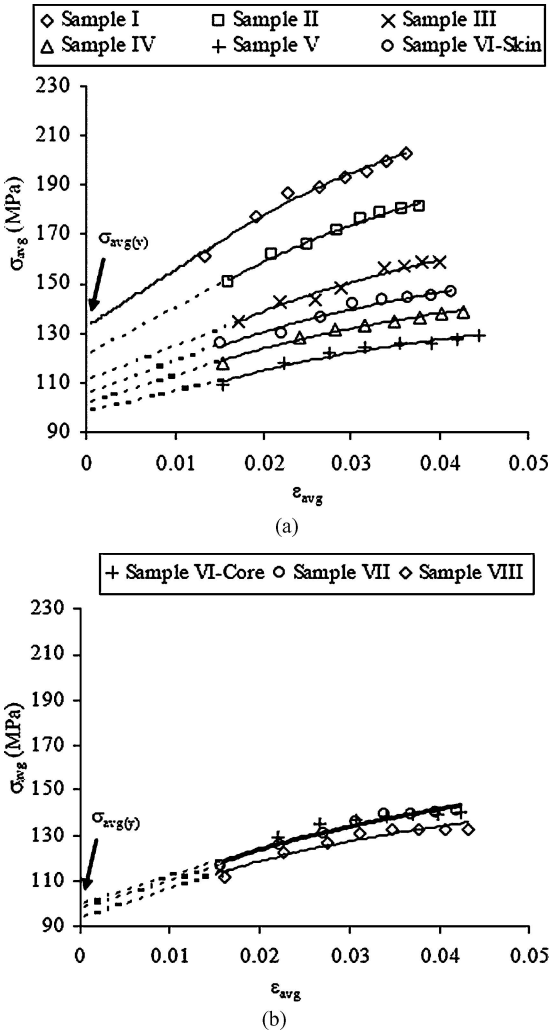

Figure 7 The calculated average indentation stress, σ_{avg}, plotted as a function of the calculated average strain, ε_{avg}, for the samples indented in the skin region (a), and in the core region (b). Constitutive relations are shown fitting the indentation data.

solidified α-Mg grains, very low in aluminum content, during the die-casting process. These α-Mg grains solidify as dendrites and are typically found in the core of the casting in regions that are close to the ingate. The remaining liquid, which is rich in aluminum, solidifies in the skin region and results in a high proportion of the intermetallic β-phase $Mg_{17}Al_{12}$ at the grain boundaries. Quantitative optical metallography was performed on one sample from the skin region, Sample II, and two samples from the core region, Samples VI-Core and VII. It was found that the skin region contained a higher percentage of grain boundaries, containing $Mg_{17}Al_{12}$, than the core region. This is in agreement with the reported findings from similar analyses performed on other die-casting magnesium alloys [24].

Analytical scanning electron microscopy performed on Samples II, VI-Core, and VII has shown that aluminum is present, for the most part, only at the grain boundaries [25]. Further, it was determined there is a higher aluminum content in α-Mg grains found in the skin region than in the core region. This study, however, explores the variation in local mechanical properties, such as σ_{avg}, in different locations, both in the skin and core regions of the magnesium die-casting component, with local changes in the grain size.

5.2. Grain size of AM60B

The average grain sizes, d, reported in this study (Table II), obtained from optical microscopy and digital image analysis, range from 4.8 μm in the skin region, to 14.9 μm in the core region. There is, also, a larger variability in the grain size measurements in the core region compared to the skin region (Fig. 4). The average d through the entire skin region and the core region of multiple die-castings, made under the same conditions, is 6.2 μm and 13.9 μm, respectively [20]. These grain sizes are similar to what has been previously reported for AM60B die-castings [5, 26]. The weaknesses of using optical microscopy and digital image analysis to assess the grain size are summarized by Bowles *et al.* [27], in which the authors use electron back scattered diffraction (EBSD) to determine the grain size of AZ91 and AM60 castings. The grain boundaries of magnesium-aluminum high-pressure die cast alloys are difficult to etch and some boundaries may be missed by optical analysis [27, 28]. However, the use of EBSD is not an industry standard due to the time consumption of data collection and sample preparation [27]. If the assumption that optical microscopy and digital image analysis overestimates the grain size [28] is taken

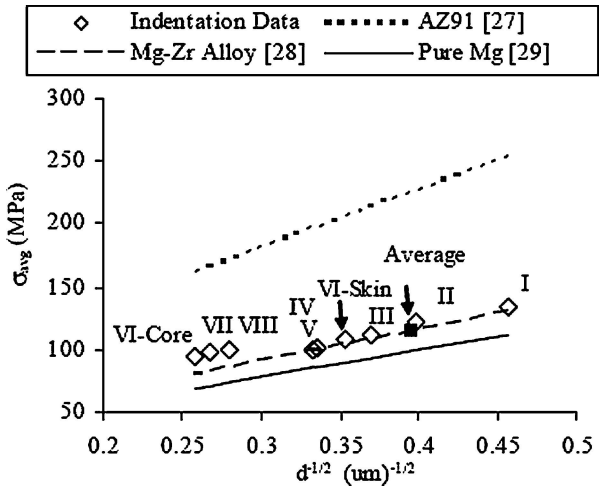

Figure 8 $\sigma_{avg(y)}$ plotted as a function of $d^{-1/2}$ in comparison with published results on similar Mg alloys. The slope of each line gives the Hall-Petch slope, k. The intercept with the flow stress axis gives the Hall-Petch intercept stress, σ_o. The results from the skin region closely follow the Hall-Petch relationship [28] while the results from the core region do not.

into account, a Hall-Petch relationship will still exist between the flow-stress and the EBSD grain size, however, the magnitude of the Hall-Petch parameters, as described below, will vary compared to the parameters determined from the optical grain sizes. Nevertheless, the dependence of the Hall-Petch parameters upon strain will be the same regardless of the method used to measure the grain size. This is described in more detail in the following sections.

5.3. Hall-Petch relationship for $\sigma_{avg(y)}$

Although Fig. 8 does show the $\sigma_{avg(y)}$ is related to the grain size according to the Hall-Petch equation in the skin region, we investigate in more detail the parameters of the Hall-Petch equation for the die-cast magnesium alloy AM60B. Fig. 8 also shows previously published results for pure magnesium and similar magnesium alloys [29–31]. Both Hall-Petch parameters: the slope, k and the intercept stress, σ_o, can be calculated from this plot. The Hall-Petch slope, k, is 274 MPa-μm$^{-1/2}$ and the intercept stress, σ_o, is 10 MPa (R^2 = 0.98) for the data from this investigation. These values compare quite well with reported values in the literature, as shown in Fig. 8. The Hall-Petch parameters of pure magnesium [31] during tensile testing are reported as $k = 220$ MPa-μm$^{-1/2}$, and $\sigma_o = 12$ MPa, while for magnesium alloyed with small amounts of zirconium, $k = 250$ MPa-μm$^{-1/2}$, and $\sigma_o = 18$ MPa [30]. Therefore, the Hall-Petch equation and parameters obtained for the die-cast magnesium alloy AM60B from spherical indentation testing in the skin region accurately reflect reported values in literature.

The results in Fig. 8 from the core region do not follow the same Hall-Petch relationship, as do the results from the skin region. Several explanations for these results are possible, including the fact that the microstructure between the skin and the core regions is different as discussed above. The variability in the observed grain size in the core region (see Fig. 4) may introduce significant uncertainty in the actual average grain size. The spherical indenter may come into contact with several grains that do not represent the "average" grain size (as shown in Table II). Further study in this area is currently underway.

5.4. Hall-Petch relationship for plastic straining

The Hall-Petch slope, k, for increasing values of plastic strain can be theoretically shown to increase in the case where local plastic strain is dependent upon the density of geometrically necessary dislocations [32]. This dislocation density is necessary to accommodate the strain incompatibility in small grains with different crystallographic orientation. This relationship is not observed, however, with large (10–50 μm) grain size aluminum-based alloys tested over a wide plastic strain range (1–16%) [32]. The Hall-Petch slope has also been reported to decrease with increasing strain over larger values of plastic strain for polycrystalline Cu (grain sizes 12–90 μm, strain up to 40%) [33, 34].

The Hall-Petch slope, k, can be determined as follows for this study. The average indentation stress, σ_{avg}, at a given plastic strain can be determined directly from the σ_{avg} vs. ε_{avg} plot in Fig. 7. The indentation stress, σ_{avg}, was calculated as a function of $d^{-1/2}$ for several levels of plastic straining (0.02, 0.03 and 0.04, the plastic strain range of testing completed in this study) determined from indentation testing, for the skin region, from which the Hall-Petch parameters k and σ_o can then be determined from each level of plastic straining. The Hall-Petch slope, k, is shown in Fig. 9 plotted as a function of $\varepsilon_{avg}{}^{1/2}$. The k values show a linearly increasing trend with an increasing $\varepsilon_{avg}{}^{1/2}$ over the plastic strain range tested in this study. This is expected based upon the shape of the flow curves in Fig. 7. It should be noted that these curves are the result of multiple indentation tested (four indentation tests per curve). Very littler scatter exists in the resulting curves and this validates the trends shown by the data in Fig. 9. This finding is supported by the theory of geometrically necessary dislocations, which states that k should increase with plastic strain. One must keep in mind, however,

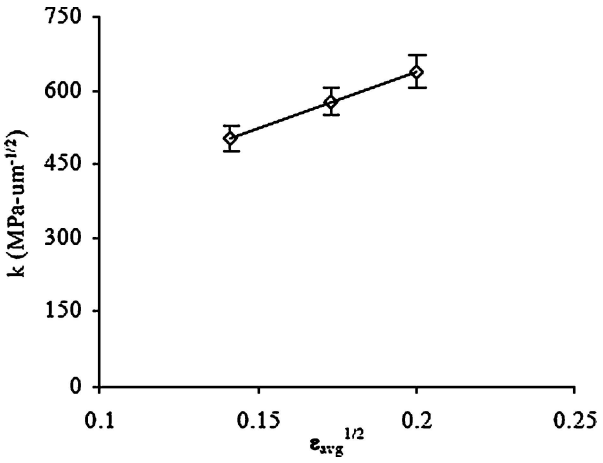

Figure 9 σ_{avg} plotted as a function of $\varepsilon^{1/2}$, encountered during indentation testing. The plot shows a linear relation between k and $\varepsilon^{1/2}$.

that the plastic strain range tested in this study is small (2–4%) and therefore it does not allow for any firm conclusions to be drawn regarding the details of the relation between plastic deformation and dislocation density. The plastic deformation of magnesium-based die-casting alloys is a complex process that requires further study.

6. Conclusions

Spherical indentation testing was performed on five samples from the skin region, two samples in the core region and one sample on both the skin and core regions of the die cast magnesium alloy AM60B. The average measured grain size of each sample varied from 4.8 to 9.0 μm in the skin region and from 12.7 to 14.9 μm in the core region of the casting.

We conclude that the flow stress of AM60B depends upon average grain size according to the Hall-Petch equation in the skin region. It is suggested that differences in the microstructure affect the indentation results from the core region; however, this dependence requires further experimental work. We observe that the Hall-Petch slope, k, increases with increasing plastic strain, however, this observation is limited by the small range of plastic strain in this study, and therefore, does not allow for any firm conclusions to be drawn. The Hall-Petch slope and the intercept stress at the yield point, calculated from the spherical indentation data in the skin region are similar in magnitude to the published results obtained from uniaxial testing.

Acknowledgements

This research is funded by Meridian Technologies and the AUTO21 Network of Centres of Excellence, an automotive research and development program focusing on issues relating to the automobile in the 21st century. AUTO21, a member of the Networks of Centres of Excellence of Canada program is funded by the Natural Sciences and Engineering Research Council (NSERC), the Social Science and Humanities Research Council (SSHRC) and multiple industry and government partners.

References

1. E. O. HALL, *Proc Phys. Soc.* **B64** (1951) 747.
2. N. J. PETCH, *J. Iron Steel Inst.* **174** (1953) 25.
3. E. O. HALL, *Nature* **173** (1954) 948.
4. Z. SHAN and A. M. GOKHALE, *Mater. Sci. Engg.* **A361** (2003) 267.
5. D. RODRIGO, M. MURRAY, H. MAO, J. BREVICK, C. MOBLEY and R. ESDAILE, in Proceedings of the 20th International NADCA Congress, World of Die Casting (NADCA, Cleveland, OH, 1999) p. 219.
6. A. WAHLBERG, *J. Iron Steel Inst.* **59** (1901) 243.
7. H. O'NEILL, *Proc. Inst. Mech. Eng.* **151** (1944) 116.
8. D. TABOR, in "The Hardness of Metals" (Clarendon Press, Oxford, United Kingdom, 1951) pp. 12, 46.
9. K. L. JOHNSON, *J. Mech. Phys. Sol.* **18** (1970) 115.
10. S. D. MESAROVIC and N. A. FLECK, *Proc. Royal Soc. Lond., Series A* **455** (1999) 2707.
11. J.-H. AHN and D. KWON, *J. Mater. Res.* **16** (2001) 3170.
12. M. BEGHINI, L. BERTINI and V. FONTANARI, *Intern. J. Comp. Appl. Technol.* **15** (2002) 168.
13. F. M. HAGGAG, U.S. Patent #4852397 (1990).
14. Y. Y. LIM and M. M. CHAUDHRI, *Philos Mag. A.* **82** (2002) 2071.
15. M. FURUKAWA, Z. HORITA, M. NEMOTO, R. Z. VALIEV and T. G. LANGDON, *Acta Mater.* **44** (1996) 4619.
16. A. COUTURE and J. W. MEIER, Mines Bran. Res. Rep. R 153. (Canada Department of Mines and Technical Surveys, 1965), p. 1.
17. T. M. YUE, H. U. HA and N. J. MUSSON, *J. Mater. Sci.* **30** (1995) 2277.
18. W. C. OLIVER and G. M. PHARR, *J. Mater. Res.* **7** (1992) 1564.
19. J. ALCALA, A. C. BARONE and M. ANGLADA, *Acta Mater.* **48** (2000) 3451.
20. D. YIN, in "Microstructural characterization of a magnesium die-casting", M.E.Sc. Thesis (University of Western Ontario, London, Ontario, 2004).
21. B. J. COULTES, in "Mechanical Property Variation in a Magnesium High-pressure Die-cast Component", M.E.Sc. Thesis (University of Western Ontario, London, Ontario, 2004).
22. B. J. COULTES, J. T. WOOD, G. WANG and R. BERKMORTEL, in "Magnesium Technology 2003", edited by H. I. Kaplan (TMS, Warrendale, PA, 2003) p. 45.
23. G. MIMA and Y. TANAKA, *J. Jpn. Inst. Met.* **35** (1971) 319.
24. W. P. SEQUEIRA, G. L. DUNLOP and M. T. MURRAY, in Proceedings of the 3rd International Magnesium Conference, edited by G. W. Lorimer (The Institute of Metals, Manchester, UK, 1996) p. 63.
25. J. P. WEILER, J. T. WOOD, R. J. KLASSEN, R. BERKMORTEL and G. WANG, in "Magnesium Technology 2005", edited by N. R. Neelameggham, H. I. Kaplan and B. R. Powell (TMS, Warrendale, PA, 2005) p. 191.
26. B. E. CARLSON, in "The Effects of Strain Rate and Temperature on the Deformation of Die Cast AM60B (950425)" (SAE, 1995) p. 343.
27. A. L. BOWLES, J. R. GRIFFITHS, and C. J. DAVIDSON, in "Magnesium Technology 2001", edited by J. Hryn (TMS, Warrendale, PA, 2001) p. 161.
28. T. WEISS and P. DAVIES, *Trans. Inst. Metal Finish.* **78** (2000) 65.
29. T. ABBOTT, M. EASTON and W. SONG, *Mater. Sci. Forum.* **419–422** (2003) 141.
30. P. ANDERSSON, C. H. CACERES and J. KOIKE, *ibid.* **419-422** (2003) 123.
31. F. E. HAUSER, P. R. LANDON and J. E. DORN, *Trans. Amer. Inst. Min. Metall. Petrol. Eng.* **206** (1956) 589.
32. D. J. LLOYD and S. A. COURT, *Mater Sci Technol* **19** (2003) 1349.
33. U. F. KOCKS, *Metall. Trans.* **1** (1970) 1121.
34. R. P. CARREKER and W. R. HIBBARD, *Acta. Metall.* **1** (1953) 654.

Received 30 November 2004
and accepted 31 March 2005